Interfacial roughening during solid phase epitaxy: Interaction of dopant, stress, and anisotropy effects

William Barvosa-Carter[a] and Michael J. Aziz[b]
Division of Engineering and Applied Sciences, Harvard University, Cambridge, Massachusetts 02138

A.-V. Phan
Department of Mechanical Engineering, University of South Alabama, Mobile, Alabama 36688–0002

T. Kaplan and L. J. Gray
Oak Ridge National Laboratory, Oak Ridge, Tennessee 37830

(Received 7 October 2003; accepted 19 July 2004)

The effects of externally applied stress and rate-enhancing dopants on interfacial roughness during the solid phase epitaxial growth of ion-implantation-doped Si are investigated using cross-sectional transmission electron microscopy and time-resolved reflectivity. We find long-wavelength roughness in the absence of an applied stress that arises solely from the dopant-gradient. With the addition of a compressive stress, the interface roughens further with an enhanced magnitude and a dramatically reduced wavelength. We discuss the experimental results in the context of a simulation that includes our current understanding of stress, dopant-gradient, and interface anisotropy effects. We find a rich interplay between these effects in determining growth morphology evolution, and demonstrate the successes and current limitations of the model. © *2004 American Institute of Physics*. [DOI: 10.1063/1.1790580]

I. INTRODUCTION

Si-based devices can be greatly enhanced through alloying with Ge and the imposition of an extrinsic strain.[1–3] While such devices can be readily made using molecular beam epitaxy (MBE), their formation using a conventional ion-implantation followed by amorphization and solid phase epitaxial growth (SPEG) is strongly limited by interface breakdown and defect generation. For example, during SPEG in the Si–Ge system, roughening of the amorphous-crystal (*a-c*) interface occurs above a Ge content of 3–7 at.%, followed by the generation of dislocations and stacking faults, leading to a severely degraded material not suitable for devices. This roughening is not fully understood, but is thought to result from a complex interplay of local interface stress, composition, and orientation (growth kinetic anisotropy) effects.[4] However, in the past, researchers had difficulty in isolating these different elements in the strained Si–Ge system.

In this work, we explore a possible avenue for decoupling the effect of strain from those of composition and interface orientation, examining them additively in a controlled manner in an effort to understand their interaction and influence on interface evolution. We examine the problem both experimentally and through phenomenological modeling. On the experimental side, we study the SPEG of B-doped amorphous Si(a-Si) on crystalline Si(c-Si) as a proxy to mimic the rate-enhancing effect of Ge.[5] Instead of a self-stress arising from the presence of Ge, which does not arise from the addition of B, stress is applied mechanically. Because we can achieve similar stress states to those that would be imposed by the substrate during SPEG of amorphous Si–Ge alloy thin films, we can therefore introduce stress as an external, independently controlled variable. Additionally, we seek a phenomenological model that can combine the individual factors of stress,[6,7] rate-enhancing dopants or alloying elements,[5,8] and growth kinetic anisotropy[9] and examine their interaction in relation to the experimental data.

Our experimental results show that B-doped a-Si is promising for approximating the observed behavior in SPEG of Si–Ge and permits the separate examination of the individual roles, that stress, composition, and orientation play during morphological evolution. For example, we observe that composition alone can destabilize the interface during SPEG of B-doped Si, in a manner similar to that observed in Si–Ge.[8] When stress is externally applied, interface roughness evolution is observed similar to that in the strained Si–Ge system: increasing the stress leads to an increasing roughness and a dramatic decrease in lateral length scale.

Comparing our model with the experiment, we find a rich interplay between stress, dopant-gradient, and crystalline anisotropy effects in determining the growth morphology evolution. In particular, we find success in modeling the combined effects of any two out of these three factors. For instance, we have previously shown a successful agreement with experiment when modeling combined stress and composition effects for flat interfaces,[10] and when modeling combined stress and orientation effects for constant composition structures.[6,7] In this current work, we successfully model the combined composition and orientation effects at zero stress. However, when all three effects are present, as in the current experiment or in Si–Ge, our model diverges qualitatively from the observed behavior. We discuss the successes and limitations of this modeling approach and suggest future

[a]Present address: HRL Laboratories, Malibu, CA; electronic mail: wbc@hrl.com
[b]Electronic mail: maziz@harvard.edu

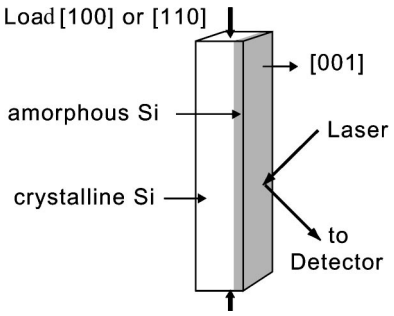

FIG. 1. Experimental geometry.

work. It is anticipated that these same effects will be important in some scenarios involving deposition from a vapor, but despite the vast amount of literature devoted to processes such as MBE, to our knowledge, there has been no exploration of these issues in that arena.

II. EXPERIMENT

The sample geometry and procedure used to measure the in-plane stress effects on SPEG of Si has been described in detail elsewhere.[7] The samples for this study consisted of a-Si layers produced on 0.034-in.-thick, double-side-polished (001) silicon wafers by ion implantation ($^{28}Si^{+}$, $1\times10^{15}/cm^2$ at 60 keV followed by $2\times10^{15}/cm^2$ at 180 keV and $^{11}B^{+}$, $5\times10^{15}/cm^2$ at 50 keV). This produced an approximately Gaussian depth distribution of B centered at ~150 nm deep in a ~320-nm-thick a-Si film. The loading and optical geometry are shown schematically in Fig. 1. In this arrangement, a uniaxial stress, σ_{11}, was applied in the plane of the amorphous-crystal interface. In most of our experiments, we applied stress along the [100] direction. A few samples were also annealed along [110], and no striking differences in behavior could be observed. Optical access enabled the real-time measurement of the growth rate using time-resolved reflectivity (TRR)[11] monitored at $\lambda = 632.8$ nm. All the samples were preannealed for 1 h at 450 °C, and then treated to varying magnitudes of stress, as described in the following section.

Figure 2 shows a series of cross-sectional transmission electron microscopy (TEM) micrographs of several samples annealed for successively longer times. The initial interface (a) is shown after the preannealing at 450 °C for 1 h. This initial interface is not completely flat but has a roughness on the order of 2–3 nm. With subsequent annealing at 500 °C and a (compressive) stress of −0.5 GPa in the plane of the interface, however, the roughness of the sample increases dramatically as in (b), reaching a peak-to-trough roughness of ~25 nm at a depth of roughly 180 nm. The third micrograph (c) shows that the interface structure at 90 nm depth is roughly the same as that at 180 nm. Relative to the zero-stress sample shown in Fig. 2(d), the interface roughness is significantly enhanced when the growth occurs under stress. Additionally, a greatly enhanced density of dislocations can be seen that span the region between the interface and the end-of-range damage left from the implantation process. We suspect that these are most likely hairpin-shaped dislocations, although no additional studies were made to determine

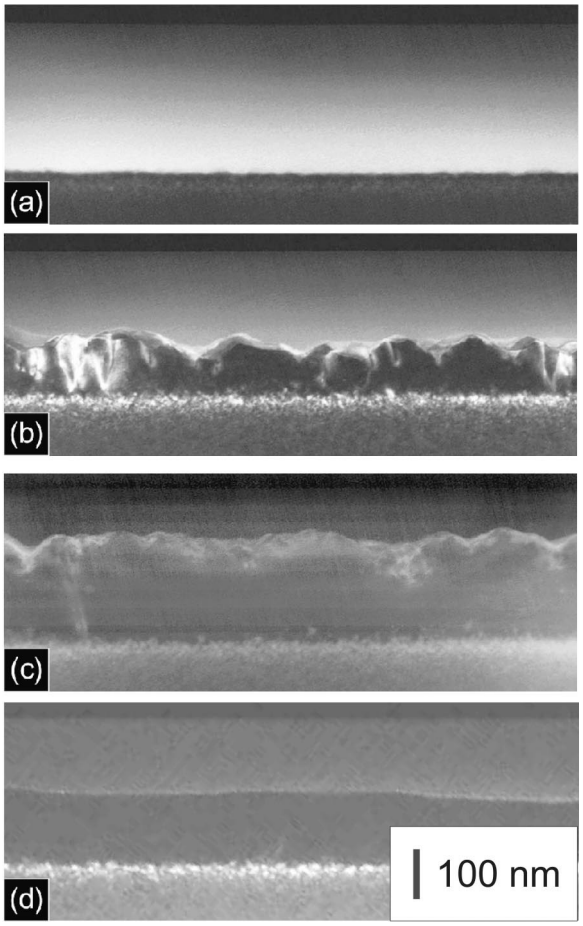

FIG. 2. Evolution of the amorphous-crystal interface: (a) initial interface; (b) after 90 nm growth under a compressive uniaxial stress of −0.5 GPa applied parallel to the interface in the plane of the page; (c) after 180 nm growth under a compressive stress of −0.5 GPa, and (d) after 150 nm growth in the absence of stress.

the character of these defects. While most end-of-range damage results in dislocation loops at this depth, which minimize the total line energy at a constant enclosed area, we surmise that these additional defects are stabilized by the applied stress, allowing them to propagate along with the growing interface at the expense of an additional line energy.

To investigate the time dependence of the evolution of the interface roughness, we annealed several stressed samples while monitoring the TRR for as much of the regrowth as possible. In this measurement, we postulate that changes in the reflectivity, away from the "ideal" case of reflectivity from a perfectly flat interface, are a direct result of scattering due to interface roughness. Interpretation of the raw reflectivity data is somewhat complicated by the fact that the interface velocity changes with time, both due to the nonuniform boron doping, as well as the differences in the applied stress. To facilitate comparison, we converted reflectivity versus time to reflectivity versus depth using the method described by McCallum.[12] The absolute reflectivity of the sample, which we seek to correlate to differences in interface roughness, is obtained from the raw data through a calibration of the reflected signal against known reflectivity standards. These curves are compared to an ideal curve (labeled "theory" in Fig. 3) calculated using the theoretical ex-

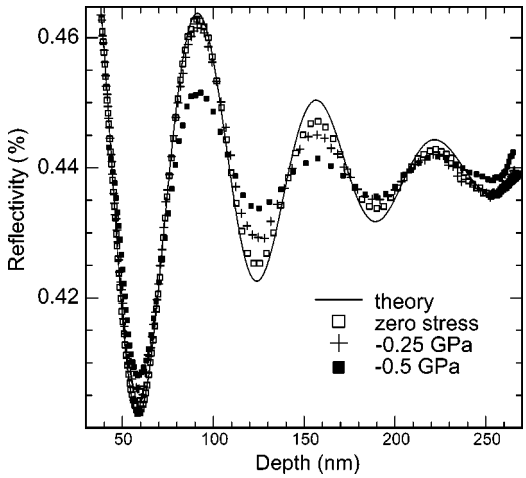

FIG. 3. Sample reflectivity vs average interface depth for $\sigma_{11}=0$ GPa, −0.25 GPa, and −0.5 GPa. Curve labeled as "theory" is for the ideal case of planar interface.

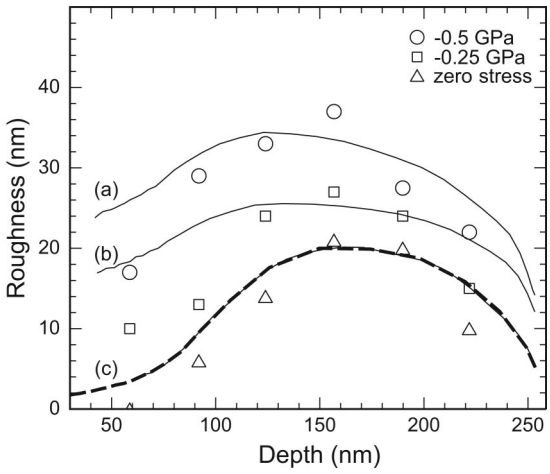

FIG. 4. Interface roughness vs depth. Data points are extracted from the reflectivity in Fig. 3. Bold dashed line: Elliman-Wong model for zero stress. Thin solid lines: Our simulated roughness evolution as described in the text using, from top to bottom, (a) $\sigma_{11}=-0.5$ GPa, $A_0=6.5$ nm; (b) $\sigma_{11}=-0.25$ GPa, $A_0=5.5$ nm; (c) $\sigma_{11}=0$ GPa, $A_0=0.72$ nm.

pression for the reflectivity of a thin a-Si film on a very thick substrate, with the temperature-dependent values for the indices of refraction quoted by Olson and Roth.[11]

Figure 3 shows a comparison of the TRR obtained from three samples annealed at stresses of 0, –0.25, and -0.5 GPa. While the 0 and −0.25 GPa samples could be completely crystallized, the −0.5 GPa sample could only be crystallized under stress within 50 nm of the surface before the sample fractured. Comparing the three experimental curves to the calculated curve in Fig. 3, the most significant feature is that the amplitude of the TRR oscillations is reduced with increasing stress.

III. ANALYSIS

Given the TEM results for the −0.5 GPa samples, it appears that the primary mechanism for the TRR amplitude reduction seen in Fig. 3 is the roughening of the *a-c* interface. We extracted the interface roughness as a function of depth from the TRR data using the method of Zeng *et al.*[13] and the implementation given by Elliman and Wong, (EW)[8] who took their measure of interface roughness as the full width of a normalized triangular distribution of the interface depths. The method assumes that the spatial periodicity of the interface roughness is much greater than the 130 nm wavelength of light in the amorphous phase. Making the opposite assumption does not change our conclusions. To extract the quantitative values of the roughness from the TRR data, we match each maximum or minimum in the TRR curve to a reflectivity predicted theoretically, assuming a symmetric triangular distribution of the interface depths with full width at full maximum A. We find that such a triangular distribution is reasonable, with other functional forms fitting the depth distribution in our micrographs less well.

Figure 4 gives values of A as a function of depth for each of the curves shown in Fig. 3. Generally, we find that A increases overall with increasing stress, and tends to follow the depth distribution of the dopant concentration. Significantly, it appears as though the "zero stress" sample has a nonzero roughness for most of the regrowth. At a microscopic level, we find that this is indeed the case, as shown in the micrograph in Fig. 5. While at short length scales [<100 nm, Fig. 2(d)] the interface is smooth, variations in interface position appear over much longer length scales ($\lambda \sim 800-1200$ nm). The interface depth on average deviates about ±10 nm, which compares favorably with the value of A, extracted from the TRR at the same depth.

The higher stress samples show an increasing interface roughening (Fig. 4). The sample held at −0.25 GPa shows a trend similar to the roughness of the zero-stress sample, in that the roughness increases until the peak of the B distribution is reached, and then, again following the decreasing B concentration, it decreases. The same trend is evident with the −0.5 GPa sample, except that after the interface passes through the peak of the boron distribution, the roughness is sustained somewhat. This is consistent with the TEM results shown in Fig. 2(c). Additionally, we find that, while there is a clear enhancement of the interface roughness ($\sim\times 1.5-2$ at −0.5 GPa), stress induces a dramatic reduction in λ.

IV. ANALYTICAL MODELING OF ROUGHNESS EVOLUTION: ZERO-STRESS CASE

For the case of the zero-stress samples, our understanding of the variations in the interface depth is in terms of a

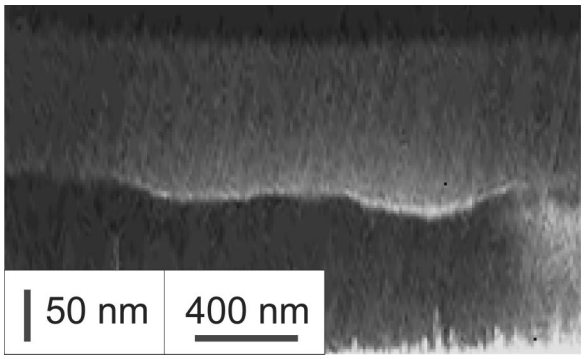

FIG. 5. Interface morphology at 150 nm depth after annealing with zero stress. To enhance the visibility of the interface corrugation, the lateral scale has been compressed by a factor of 4 relative to the vertical scale.

dopant-gradient-driven kinetic interface instability described by Elliman and Wong.[8] Their description of this process is analytical, and we present a comparison of our results to the predictions of their model. The EW interface roughening mechanism occurs when the interface is growing into a region of increasing rate-enhancing impurity content, and initially depth-displaced segments of the interface move through the impurity distribution at different times, with their relative displacement essentially being magnified by the rate enhancement. EW show that as a result, the interface roughness A scales with the velocity distribution $v(z)$ according to

$$A(z) = A(z_0)[v(z)/v(z_0)], \tag{1}$$

where z is the average depth of the interface and $A(z_0)$ is the interface roughness at an arbitrary reference depth z_0. We find that the zero-stress samples follow this relationship. In Fig. 4, we compare the zero-stress data to the EW model: the bold dashed curve is the velocity distribution extracted from the zero-stress TRR curve scaled by the interface roughness measured at a depth of ~150 nm from Fig. 5.

It is highly plausible that the occurrence of roughness only for large lateral length scales ($\lambda > 800$ nm) for the stress-free case is attributable to the crystalline anisotropy effects: v is drastically reduced as the local interface orientation tends away from (001) toward (111).[9] The orientation effect prejudices the evolution toward a slope selection and dictates a maximum attainable aspect ratio $\Gamma \equiv A/\lambda$ for interface fluctuations; hence, for a given A, there is a minimum value of λ. An additional consequence of the anisotropy effect is that an initially rough interface in the absence of stress or dopants tends to be smoothed out as faster (001) trailing segments overtake the slower, sloped segments. As a result, in the absence of stress, the EW mechanism amplifies only large λ.

V. NUMERICAL SIMULATIONS OF INTERFACE EVOLUTION

While successful for describing the small Γ roughness evolution due to composition gradient effects, the EW model does not permit us to explore the large Γ regime, nor allow intuitive inclusion of stress effects on interface roughness. A simple analytical treatment of the interface morphology due to these effects is difficult to obtain for large Γ: while the deviations from (001) and B concentration are local effects, the stress on each local segment of the interface depends on the overall morphology. To explore the complex interplay between the interacting factors of stress, dopant-gradients, and kinetic anisotropy as the interface evolves into the large Γ regime, we turn to numerical simulation techniques. Within the simulation, the local growth rate is determined by a phenomenological growth model developed previously.[6,14] This model incorporates sufficient detail to capture several possible mechanisms for interfacial roughening, including the EW-like effects due to composition gradients, growth kinetic anisotropy/orientation effects,[9] and stress effects due to the Asaro-Tiller[15]/Grinfeld[16] (ATG) instability and the stress-induced kinetically-driven instability we have described previously.[6] It is important to note that this model for the local growth rate is not atomistic in nature—we seek instead to combine phenomenological descriptions of individual effects on interface kinetics and stability.

The local interface velocity v (normal to the interface) is determined by using Eq. (1) in Ref. 14

$$v(\theta, C, \boldsymbol{\sigma}, \kappa) = v_0(\theta) f(C) \exp\left(\frac{\sigma_{ij} V_{ij}^* - E^*}{k_B T}\right) \sinh\left(\frac{\Delta G_{ac}(\boldsymbol{\sigma}, \kappa)}{2 k_B T}\right), \tag{2}$$

where θ is the interface misorientation relative to (001), C is the concentration of dopant, $\boldsymbol{\sigma}$ is the local stress tensor at the interface, κ is the local curvature of the interface, v_0 is the velocity of an undoped stress-free planar interface, $f(C)$ is discussed subsequently, $\mathbf{V}^*$ is the activation strain tensor, E^* is the activation energy, k_B is Boltzmann's constant, and ΔG_{ac} is the driving free energy, which includes contributions from capillarity, elastic strain energy density in both phases, and stress-strain work done on the surroundings. The sum over repeated Cartesian indices $i, j = 1, 2$, and 3 is implied. We refer the reader to Ref. 14 for the details. In order to take into account the rate-enhancing effects of the B distribution in $f(C)$, we directly use the measured velocity as the base velocity function as we did in the previous section. While some errors in the measurement of the velocity itself as well as errors due to the nonplanarity of the interface are introduced by this method, we avoid complications arising from needing to accurately model the rate-enhancing effects of the B distribution. We obtain similar results, albeit less well matched to the experimental data, by using instead the B depth distribution and the phenomenological descriptions previously developed[11] to predict rate enhancement due to dopant concentrations.

Stress effects on interface morphology can occur through changes in growth energetics or kinetic barriers. Significantly, we include in the function for v parameters that, with appropriate values, allow expression of both the ATG instability (through changes in ΔG_{ac}) as well as the stress-induced kinetically-driven instability through $\mathbf{V}^*$. ATG is an energetically-driven growth instability, in which interface roughening can allow a reduction in the overall elastic strain energy (due, in the case of Si–Ge SPEG, to the self-stress caused by Ge), and has previously been assumed to be the source of initial interface roughening.[4,8] In the case of SPEG of pure Si, we have previously shown that stress can destabilize the *a*-*c* interface and allow it to roughen. The mechanism for this roughening is fundamentally different than that described by ATG, arising from the effect of stress on the barriers to local kinetic growth processes[10,17] rather than the energetic concerns in ATG. In the earlier work, we determined that this kinetically-driven instability, rather than the ATG instability, was primarily responsible for the interfacial roughening during the SPEG of Si. However, because both the ATG and the stress-induced kinetically-driven instabilities are predicted to enhance the interface roughness under a compressive stress, becoming more effective at a larger Γ, we include sufficient detail to allow the expression of both in our model. The simulations are based on a coupling of the boundary contour method (BCM) and level set methods. The

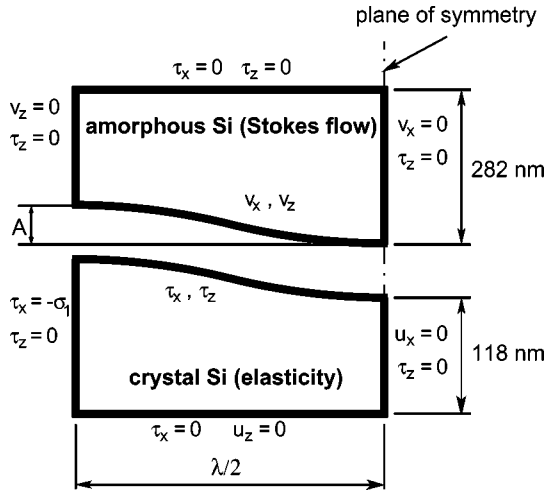

FIG. 6. Breakdown of geometry and boundary conditions for the simulation.

BCM (e.g., Ref. 18) is used to evaluate displacements and boundary stresses on the crystal interface and tractions on the amorphous interface. Level set methods track the evolution of this crystalline/amorphous interface. This work uses a narrow-band level set formulation[19] to characterize and advance the evolving interface. For details about the theory, algorithms, and applications of level set methods, the reader is referred to Ref. 20.

We consider a two-phase amorphous-Si/crystal-Si system subjected to a nonhydrostatic compressive σ_{11}. Three cases of stress, namely, $\sigma_{11}=-0.5$, -0.25, and 0 GPa, are studied. The interface of the system is initially modeled as a sine wave, as described in Fig. 6, with an imposed wavelength and an initial amplitude A_0 to be determined by a comparison between the final morphologies of experiments and simulations. Because we have so little information about the roughness spectrum before growth, the starting wavelength in the simulations was fixed at 900 nm, a value chosen somewhat arbitrarily because the results are fairly insensitive to the wavelength in this regime. By symmetry, only a half wavelength segment needs to be treated. The silicon crystal is modeled as an isotropic linear elastic solid with a shear modulus $G_c=0.6814\times10^{11}$ Pa and Poisson ratio $\nu_c=0.2174$ (Ref. 21). The amorphous solid is modeled by Stokes flow with a time-dependent viscosity to reflect structural relaxation.[14] We assume plane stress for the elastic solids analyses.

The framework employed to determine the interface growth[14] can be described as follows: At each time step of the growth simulation, the traction (normal component of the stress tensor) on the crystal interface is initially assigned its coverged value from the previous time step. Next, the crystal elasticity problem is solved using the BCM for elasticity with the new interface position. In order to obtain a solution obeying traction continuity across the interface, the flow velocity boundary condition for the viscous amorphous material at the interface must be determined. This velocity, $\mathbf{v}_a$, is evaluated as the change in the elastic displacement $\mathbf{\Delta u}$ of the crystal at each point along the interface, caused by the strain energy relaxation solved for by the BCM[22] and distributed over the growth time step Δt, by $\mathbf{v_a}=\mathbf{\Delta u}/\Delta t$. Once $\mathbf{v_a}$ is determined, the traction $\boldsymbol{\tau}_\mathbf{a}$ on the amorphous interface is found by solving the amorphous viscous flow problem using the BCM for Stokes flow. The traction on the amorphous interface at the ith iteration, $\boldsymbol{\tau}_\mathbf{a}^{(i)}$, is used to update the traction $\boldsymbol{\tau}_\mathbf{c}^{(i+1)}$ of the subsequent iteration on the crystal interface using $\boldsymbol{\tau}_\mathbf{c}^{(i+1)}=\boldsymbol{\tau}_\mathbf{c}^{(i)}+k_r\boldsymbol{\tau}_\mathbf{a}^{(i)}$, where k_r is a relaxation coefficient, and the calculation is iterated to convergence.

Upon convergence, the other components of the boundary stress tensor on the crystal interface are computed using a postprocessing BCM routine. The interface velocity v is then determined by substituting the boundary stress into Eq. (2). Finally, v is supplied to a level set package in order to advance the crystal interface for the given time step Δt.[23]

VI. SIMULATION RESULTS AND DISCUSSION

Our simulation results of the roughness (peak-to-peak amplitude A) versus depth for applied stresses of 0, -0.25, and -0.5 GPa, for both the simulation and experiment, have been presented in Fig. 4. As stated in the previous section, the only adjustable parameter in these calculations is the peak-to-valley amplitude A_0 of the initial interface corrugation, chosen to best match the evolution of the roughness, as measured in the experiment. The velocity distribution as a function of depth, the stress state, and the effects of stress are all factors fixed by the experiment. The simulation results are generally in agreement with the experimental trend of increasing stress-causing increased interface roughening.

Although we find reasonable agreement between simulation and experiment if the initial wavelength in simulation is held fixed at 900 nm, the model does not permit us to understand how the selected experimental wavelength with stress. If we consider a family of simulations in which the initially imposed wavelength is permitted to vary and the initial amplitude is held constant, the simulations appear to disagree qualitatively with the observations. In the experiment, we observe a characteristic wavelength dominating the final morphology that decreases with increasing applied compressive stress (e.g. compare Figs. 2 and 5), whereas the simulations, assuming a wavelength-independent initial amplitude, predict no such characteristic wavelength. Rather, the simulations predict a maximum roughness (i.e., at the peak of the boron profile) that is independent of wavelength for long wavelengths, with a cutoff for wavelengths below ~500 nm, as shown in Fig. 7.

In the linear regime of the model, we would expect the wavelength that exhibits the maximum amplification rate to be chosen by a competition between the various roughening and smoothening effects, which have different dependence on wavelength. We expect the dopant-gradient-induced kinetic roughening to be independent of wavelength. We expect the compressive stress to most rapidly amplify the short wavelengths, where stress concentrations are greatest, and not amplify sufficiently long wavelengths, where stress concentrations are negligible.[24] We expect kinetic anisotropy to return the interface to planarity because off-[001] orientations have lower mobilities, allowing the trailing [001] segments to "catch up" and readily overtake the off-oriented segments; for a given amplitude, this effect should be the

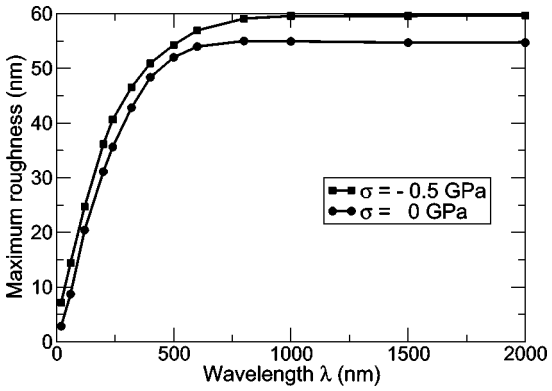

FIG. 7. Maximum roughness over the course of a simulation vs wavelength λ for an initial amplitude $A_0=2$ nm and applied stress of −0.5 and 0 GPa.

strongest at short λ, where the broadest range of orientations is exposed, and vanish at long λ. The effect of capillarity, another restoring force common to most morphological stability problems, is negligible in our case because the chemical contribution to the driving free energy ΔG_{ac} in Eq. (2) is always very large in magnitude compared to the capillary contribution. It may be that in the absence of an effect that preferably damps long-wavelength perturbations, the final roughness spectrum is very sensitive to the long-wavelength components of the initial roughness spectrum.

The cutoff at short λ in the simulations in Fig. 7 takes the form of a maximum observed aspect ratio Γ. This observation indicates that in the case of a strongly driven roughening, kinetic anisotropy may serve only to limit amplification beyond a maximum aspect ratio, rather than provide any significant restoring force for smaller aspect ratios. If, at small amplitudes, the amplifying effect of stress overwhelms the restoring force of anisotropy for small wavelengths, a kinetically selected slope and aspect ratio may result from the nonlinear turn-on of the anisotropy-induced damping at large amplitude. Hence, in a low-λ regime, there may be no mechanism for the wavelength selection. Interestingly, the amplitude cutoff predicted by the model agrees qualitatively with that observed in the experiment (compare the shoulder in the zero-stress curve in Fig. 7, ~1000 nm, with the length scale of roughening observed experimentally, 800–1200 nm in Fig. 5).

Another possible source of disagreement between the simulation and experiment could lie in the mechanics of the simulation itself. For instance, we attempt to model an inherently three-dimensional problem in a two-dimensional simulation. This was probably not a significant limiting factor in the previous studies,[6] where the primary initial structure of the interface was intentionally set by ion implantation through a patterned surface. In the present case, however, we start with a random interface structure determined by uncontrolled factors such as the initial roughness of the wafer, nonuniformities in the ion beam during amorphization, and stochastic coalescence of defects at the initial interface during the preannealing phase of the experiment. Within the model, there exists a strong, possibly nonlinear interplay between the locally defined rules for the stress-induced and dopant-gradient-induced kinetic roughening and kinetic anisotropy, factors which interact over longer length scales through the interface morphology. In a sense, the function of a simulation such as we have constructed is to help us understand the macro- or mesoscopic consequences of these microscopic rules. If the dimensionality through which these rules interact is overly constrained, anomalous behavior may result. In addition, we have further constrained the symmetry and length scale of the initial condition to a highly idealized case. It is possible that the nonlinearities in Eq. (2) imply that any simulation of the evolution of a single Fourier component will not reproduce important experimental trends. In fact, in the detailed morphologies that evolve during the simulation, we observe some nonlinearity in the distortion of the initial cosine wave with growth. If the nonlinearity is too strong, further progress may require simulation of starting profiles with experimentally determined initial roughness spectra.

Although there are factors that are not included in the simulation, such as an unknown initial roughness spectrum, a third dimension, and unknown dopant effects on off-(001) orientations, this disagreement with the experiment on the observed wavelength may indicate that a significant mechanism is absent in the simulations. Figure 2 indicates that a somewhat narrow range of λ is preferentially amplified by stress. Several alternative mechanisms may explain this effect. The foremost feature, aside from the increased interface roughness that appeared upon the application of stress, was a network of hairpin dislocations. The spatial distribution of these dislocations, and the concomitant local nonuniformities in the stress along the interface, may be responsible for choosing a wavelength. If this is indeed the case, the model for solid phase epitaxy would have to be extended to include the kinetics of dislocation generation, perhaps in a similar vein to those for the lattice-mismatched films grown from the vapor[25] or thermal stresses in growth from the melt.[26] Another possibility is that the ATG instability is more effective than our model would predict. In fact, the ATG instability has qualitative behavior that matches our observations: smaller λ should arise at increasing magnitude of stress. However, within currently accepted models for crystal growth, some factor, such as the bulk driving free energy, the interfacial energy, or the volume change upon crystallization, would need to be one or two orders of magnitude different than has been assumed, which seems unlikely.

VII. SUMMARY

Experimentally, we find that stress and dopant-gradient effects are both important in determining interface roughness evolution during the SPEG of doped a-Si layers. In the absence of stress, roughening occurs due to dopant-gradient effects. The Elliman-Wong model describes the roughening amplitude evolution quantitatively. We attribute the development of a large lateral length scale to the selective damping of short wavelengths by kinetic anisotropy. The current experimental work further shows that the application of a compressive in-plane stress causes significantly increased roughening and a dramatic decrease in lateral length scale. If the sign of either of those factors is reversed, they become sta-

bilizing, as has been shown in prior work with opposite dopant concentration gradient[10] or stress.[27] Additionally, in either case alone, this past work shows excellent agreement between our model and the experimental observations of SPEG of doped Si. In this experiment, we include both these effects when they are destabilizing.

Our experimental results are compared with a model for stress and dopant effects on the evolution of a growing amorphous-crystal interface that includes all of the phenomenological factors obtained through prior work in Refs. 6, 9, 10, 14, 22, and 27, and references therein, where all the factors are constrained aside from the amplitude of the starting interface profile. Although we find that the model can reproduce the roughness evolution versus depth and applied stress if the wavelength is held fixed, its wavelength selection versus stress is qualitatively opposite to the experiment. We hypothesize several possibilities for this discrepancy. By constraining an inherently three-dimensional problem to a two-dimensional, and/or further constraining with a single initial Fourier component, it is possible that the nonlinearities inherent in the model render the modeling approach invalid. It is also possible that some active mechanism is not present in our model, such as a nonlinear coupling between the stress and dopant factors.

ACKNOWLEDGMENTS

The authors gratefully acknowledge stimulating discussions with G. Olson, J. A. Roth, and J. Kysar. The research at Harvard was supported by NSF Grant No. DMR-0213373. The research at ORNL was supported in part by the Applied Mathematical Sciences Research Program of the Office of Mathematical, Information, and Computational Sciences, US Department of Energy under Contract No. DE-AC05-00OR22725 with UT-Battelle. One of the authors (A.-V.P.) acknowledges the support from the University of South Alabama Research Council.

[1]W. Lu, S. J. Koester, X.-W. Wang, J. O. Chu, T.-P. Ma, and I. Adesida, J. Vac. Sci. Technol. B **18**, 3488 (2000).
[2]L. E. Larson, J. Vac. Sci. Technol. B **16**, 1541 (1998).
[3]H. Presting, J. Konle, M. Hepp, H. Kibbel, K. Thonke, R. Sauer, E. Corbin, and M. Jaros, Opt. Eng. **39**, 2624 (2000).
[4]F. Corni, S. Frabboni, R. Tonini, and G. Ottaviani, J. Appl. Phys. **79**, 3528 (1996).
[5]T. E. Haynes, M. J. Antonell, C. A. Lee, and K. S. Jones, Phys. Rev. B **51**, 7762 (1995).
[6]W. Barvosa-Carter M. J. Aziz, L. J. Gray, and T. Kaplan, Phys. Rev. Lett. **81**, 1445 (1998).
[7]W. Barvosa-Carter and M. J. Aziz, Mater. Res. Soc. Symp. Proc. **441**, 75 (1997).
[8]R. G. Elliman and W. C. Wong, Appl. Phys. Lett. **69**, 2677 (1996).
[9]L. Csepregi, E. F. Kennedy, J. W. Mayer, and T. W. Sigmon, J. Appl. Phys. **49**, 3906 (1978).
[10]W. Barvosa-Carter and M. J. Aziz, Appl. Phys. Lett. **79**, 356 (2001).
[11]G. L. Olson and J. A. Roth, in *Handbook of Crystal Growth*, edited by D. T. J. Hurle (Elsevier, North Holland, 1994), Chap. 7, Vol. 3.
[12]J. C. McCallum, Appl. Phys. Lett. **69**, 925 (1996).
[13]X. Zeng, T.-C. Lee, J. Silcox, and M. O. Thompson, Mater. Res. Soc. Symp. Proc. **321**, 503 (1994).
[14]A.-V. Phan, T. Kaplan, L. J. Gray, D. Adalsteinsson, J. A. Sethian, W. Barvosa-Carter and M. J. Aziz, Modell. Simul. Mater. Sci. Eng. **9**, 309 (2001).
[15]R. J. Asaro and W. A. Tiller, Metall. Trans. **3**, 1789 (1972).
[16]M. A. Grinfeld, Sov. Phys. Dokl. **31**, 831 (1986).
[17]M. J. Aziz, P. C. Sabin, and G. Q. Lu, Phys. Rev. B **44**, 9812 (1991).
[18]A. V. Phan, S. Mukherjee, and J. R. R. Mayer, Comput. Mech. **20**, 310 (1997); A.-V. Phan, L. J. Gray, T. Kalpan, and T.-N. Phan, *ibid.* **28**, 425 (2002).
[19]D. Adalsteinsson and J. A. Sethian, J. Comput. Phys. **118**, 269 (1995).
[20]J. A. Sethian, *Level Set Methods and Fast Marching Methods* (Cambridge University Press, Cambridge, 1999).
[21]A. Witvrouw and F. Spaepen, J. Appl. Phys. **74**, 7154 (1993).
[22]The velocity due to the rate of phase transformation from amorphous to crystal, Eq. (2), does not directly affect the viscous material because material is changing identity from amorphous to crystal, but not moving. The effects of the exceedingly small volume change during the phase transformation are already included in the measured values used for v_0. The rate of phase transformation affects the flow velocity boundary condition only indirectly through the shape change that occurs during crystal growth
[23]Note that the mesh of the new interface provided by level set methods could be highly nonuniform. This nonuniformity arises as a result of the fixed grid Eulerian setting employed by level set methods, where two nodes on a new front can be very close to each other. However, this nonuniform mesh can directly be employed by the BCM without degenerating the resulting accuracy, as all the boundary integrals are evaluated analytically in the BCM for the 2D calculations.
[24]P. W. Voorhees and M. J. Aziz, in *Interfaces for the Twenty-First Century: New Research Direction in Fluid Mechanics and Materials Science*, edited by M. K. Smith, M. J. Miksis, G. B. McFadden, G. P. Neitzel, and D. R. Canright (Imperial College Press, London, 2002), p. 167.
[25]C. W. Leitz, M. T. Currie, A. Y. Kim, J. Lai, E. Robbins, E. A. Fitzgerald, and M. T. Bulsara, J. Appl. Phys. **90**, 2730 (2001).
[26]X. A. Zhu and C. T. Tsai, J. Appl. Phys. **88**, 2295 (2000).
[27]J. F. Sage, W. Barvosa-Carter and M. J. Aziz, Appl. Phys. Lett. **77**, 516 (2000).